Magnetic Resonance Imaging 57 (2019) 337–346

Contents lists available at ScienceDirect

Magnetic Resonance Imaging

journal homepage: www.elsevier.com/locate/mri

Original contribution

Diffusion kurtosis imaging of endometrial carcinoma: Correlation with histopathological findings

Ichiro Yamada[a,*], Junichiro Sakamoto[b], Daisuke Kobayashi[c], Naoyuki Miyasaka[d], Kimio Wakana[d], Noriko Oshima[d], Akira Wakabayashi[d], Yukihisa Saida[a], Ukihide Tateishi[a], Yoshinobu Eishi[c]

[a] Department of Diagnostic Radiology and Nuclear Medicine, Graduate School, Tokyo Medical and Dental University, Tokyo, Japan
[b] Department of Oral and Maxillofacial Radiology, Tokyo Medical and Dental University, Tokyo, Japan
[c] Department of Human Pathology, Tokyo Medical and Dental University, Tokyo, Japan
[d] Department of Comprehensive Reproductive Medicine, Tokyo Medical and Dental University, Tokyo, Japan

ARTICLE INFO

Keywords:
Endometrial carcinoma
Uterus
Lymph node
Diffusion kurtosis imaging
Diffusion-weighted imaging
MR imaging

ABSTRACT

Purpose: In this study, we aimed to determine the usefulness of diffusion kurtosis imaging (DKI) as a noninvasive method for the evaluation of tumor invasion depth, histological grade, and lymph node metastasis in patients with endometrial carcinoma (EMC).

Materials and methods: Our institutional review board approved this retrospective study and waived informed consent. In total, 24 patients suspected of having EMC were examined by a 1.5-T magnetic resonance imaging. DKI data were obtained using a single-shot echo-planar imaging sequence with four b values (0, 500, 1000, and 2000 s/mm^2). Kurtosis (K), diffusivity (D), and apparent diffusion coefficient (ADC) maps were generated and compared with histopathological findings.

Results: K maps from all patients identified the junctional zone as a distinct high-K zone (1.443 ± 0.362). This zone was significantly different from the zone of endometrium and outer myometrium (0.678 ± 0.179 and 0.694 ± 0.113, respectively; $P < 0.001$). K and D values of all EMCs were significantly different from those of all normal uterine wall layers. K and D values were significantly correlated with histological grades of endometrioid adenocarcinomas ($r = 0.799$, $P < 0.001$ and $r = -0.799$, $P < 0.001$, respectively), while ADC values were not ($r = -0.243$, $P = 0.382$). Metastatic and nonmetastatic lymph nodes showed significantly different K ($P = 0.001$) and D ($P = 0.001$) values, but not ADC values ($P = 0.827$).

Conclusions: DKI may be clinically useful for the noninvasive evaluation of depth of tumor invasion, histological grade, and lymph node metastasis in patients with EMC.

1. Introduction

Endometrial carcinoma (EMC) is one of the most common, fatal gynecological malignant neoplasms globally [1]. Important prognostic indicators of EMC include the International Federation of Gynecology and Obstetrics (FIGO) stage, histological subtype and grade, lymphovascular invasion, and presence of lymph node metastasis [2,3]. Specifically, the depth of myometrial invasion, histological grade, and presence of lymph node metastasis of EMCs are strong prognostic factors for patient survival rates [2–4]. Thus, accurate preoperative assessment of tumor invasion depth, histological grade, and lymph node metastasis evidently affects the selection and planning of optimal treatment for patients with EMC.

Magnetic resonance imaging (MRI) is widely used to evaluate the aggressiveness of EMC, including its myometrial invasion and metastases to lymph node and other distant sites [5–7]. However, accurate preoperative assessment of these prognostic factors is often difficult with conventional MRI. Notably, although histological grade correlates with other prognostic factors and provides critical information for treatment selection, accurate prediction of the histological grade of EMCs remains challenging without performing a needle biopsy [8–14].

Diffusion kurtosis imaging (DKI) findings are reportedly associated with histological grades of gliomas and prostate and breast cancers [15–19]. Recently, Yamada et al. [20] have demonstrated that DKI was

* Corresponding author at: Department of Diagnostic Radiology and Nuclear Medicine, Graduate School, Tokyo Medical and Dental University, 1-5-45 Yushima, Bunkyo-ku, Tokyo 113-8519, Japan.
E-mail address: yamada.crad@tmd.ac.jp (I. Yamada).

https://doi.org/10.1016/j.mri.2018.12.009
Received 3 November 2018; Received in revised form 22 December 2018; Accepted 22 December 2018

useful for the preoperative evaluation of histological grade and lymph node metastasis in patients with oral carcinoma. To the best of our knowledge, no studies have reported the use of DKI to evaluate tumor invasion depth, histological grade, and lymph node metastasis in patients with EMC, which are the most important prognostic indicators.

Therefore, we aimed to assess the usefulness of DKI as a noninvasive method for evaluating tumor invasion depth, histological grade, and presence of lymph node metastasis in patients with EMC.

2. Materials and methods

2.1. Study population

This study was approved by our institutional review board, and the requirement of written informed consent was waived owing to the retrospective study design. In total, 24 consecutive patients who were suspected of having EMC and who were surgically treated at our institution were enrolled. Mean (± standard deviation) patient age at the time of MRI was 59.5 (± 11.0) (34–86) years. After surgery, 22 of the 24 patients were histologically confirmed as having EMC and the remaining 2 patients as having atypical endometrial hyperplasia. All patients underwent preoperative MRI, including DKI.

2.2. Imaging technique

DKI was performed using a 1.5-T MRI system (Intera Achieva; Philips, Best, the Netherlands) equipped with actively shielded gradients with a maximum strength of 33 mT/m. A 32-channel phased-array body coil was used for all measurements.

DKI data were obtained in the axial plane using a spin echo-based, single-shot, echo-planar imaging sequence with the following parameters: repetition time (TR), 5000 ms; echo time (TE), 82 ms; field of view (FOV), 300 × 300 mm; matrix, 128 × 102; section thickness, 5 mm with a 0.5-mm intersection gap; and number of excitations, 6. Motion-probing gradients were applied in three orthogonal directions with four different b values (0, 500, 1000, and 2000 s/mm^2). DKI acquisition time was 5 min 5 s.

The standard MRI protocol for EMC patients at our institution included sagittal T2-weighted imaging (T2WI) (TR/TE, 2500/80 ms; FOV, 220 × 220 mm; matrix, 320 × 320; section thickness, 5 mm); axial T1-weighted imaging (T1WI) in dual echoes (TR/TE, 182/2.3 and 4.6 ms; FOV, 300 × 300 mm; matrix, 304 × 304; section thickness, 5 mm); axial DKI (mentioned above); axial T2WI (TR/TE, 4894/100 ms; FOV, 300 × 300 mm; matrix, 352 × 352; section thickness, 5 mm); and axial fat-suppressed T1WI (TR/TE, 4.7/2.3 ms; FOV, 300 × 300 mm; matrix, 272 × 272; section thickness, 5.5 mm). After intravenous bolus injection of 0.1 mmol/kg gadobutrol (Gadovist; Bayer Yakuhin, Osaka, Japan), we also performed axial triple-phase dynamic contrast-enhanced imaging (DCEI) (TR/TE, 4.8/2.4 ms; FOV, 300 × 300 mm; matrix, 288 × 288; section thickness, 5.5 mm) and sagittal CE T1WI (TR/RE, 4.7/2.4 ms; FOV, 220 × 220 mm; matrix, 304 × 304; section thickness, 4.5 mm).

2.3. Image processing

According to the DKI theory [21,22], signal intensity (SI) decay was analyzed and DKI parameters were calculated for each voxel using the following equation:

$$S = S_0 \cdot \exp(-b \cdot D + b^2 \cdot D^2 \cdot K/6)$$

where, S_0 and S are SIs at a b value of 0 s/mm^2 and at b values other than 0 s/mm^2, respectively; K indicates kurtosis (arbitrary units [a.u.]); and D indicates diffusivity ($\times 10^{-3}$ mm^2/s). K represents the deviation from the Gaussian behavior, and D represents diffusion coefficient corrected for non-Gaussian bias [21,22]. Conventional apparent diffusion coefficient (ADC) was also calculated for each voxel using the following equation: $S = S_0 \cdot \exp(-b \cdot ADC)$.

K, D, and ADC maps were generated using SIs on a pixel-by-pixel basis at b values of 0, 500, 1000, and 2000 s/mm^2. All images were processed using an in-house program developed with MatLab software (R2015a; MathWorks, Natick, MA) [20,23].

2.4. Image analysis

Two observers (I.Y. and N.M. with respectively 26 and 22 years of experience in reading MR images), who were blinded to histological findings, independently evaluated MR images for each patient. Disagreements on any findings were resolved through discussion till consensus was achieved. MR images were reviewed for the presence, SI, uniformity, and thickness of each layer of the normal uterine wall. MR images of EMCs were reviewed in terms of their presence, SI, contour, and size. Furthermore, the depth of EMC into the uterine wall was assessed according to the deepest invaded layer.

For K, D, and ADC maps, regions of interest (ROIs), which were approximately equivalent in size to the uterine wall layer thickness, tumor cross-sectional area, and lymph node cross-sectional area, were drawn by one observer (I.Y.) on the uterine wall layers, tumors, and lymph nodes, respectively, using T1WI, T2WI, diffusion-weighted imaging (DWI), and DCEI as references. Using the ImageJ 1.47 software program (National Institutes of Health, Bethesda, MD), mean values of all three or four ROIs were calculated for each uterine wall layer, tumor, and lymph node. Values of EMCs were obtained from three-dimensional volumes comprising three or four slices depending on tumor size to give full tumor coverage.

Finally, MRI findings of all patients were compared with the corresponding histopathological findings, which served as the reference standard.

2.5. Histological preparation and examination

After surgery, each surgical specimen, including the uterus, EMCs, and lymph nodes, was subjected to histopathological examination. Histological specimens were embedded in paraffin and sectioned with a microtome into 3-μm-thick slices. After staining with hematoxylin–eosin (H–E), an experienced pathologist (D.K. with 19 years of experience in histopathology), who was blinded to MRI findings, evaluated all specimens to assess the uterine wall layers and to determine the depth of tumor invasion. The pathologist classified the histological grade of EMCs according to the criteria of the FIGO grading system [2,24] as follows: grade 1 (well differentiated); grade 2 (moderately differentiated); or grade 3 (poorly differentiated), and the presence or absence of lymph node metastasis was determined.

2.6. Statistical analysis

Mean ± SD of K, D, and ADC values for the uterine wall layers, EMCs, and lymph nodes were calculated. Differences in K, D, and ADC values of the uterine wall layers and EMCs were statistically analyzed using Dunnett's test. Correlations of histological grades of EMCs with K, D, and ADC values were assessed by Spearman's rank correlation coefficient. K, D, and ADC values were compared between metastatic and nonmetastatic lymph nodes using Mann–Whitney *U* test.

The utility of K, D, and ADC values to differentiate histological grades of EMCs and to differentiate metastatic from nonmetastatic lymph nodes was compared and assessed using receiver operating characteristic (ROC) curve analyses. For ROC curve analyses, the optimal threshold of each parameter was determined as the value that would maximize the average sensitivity and specificity. Data were analyzed using IBM SPSS Statistics (Version 20; IBM SPSS Japan, Tokyo, Japan) and MedCalc (Version 17.9.7; MedCalc Software, Ostend, Belgium). A P-value of < 0.05 was considered as indicative of statistical significance.

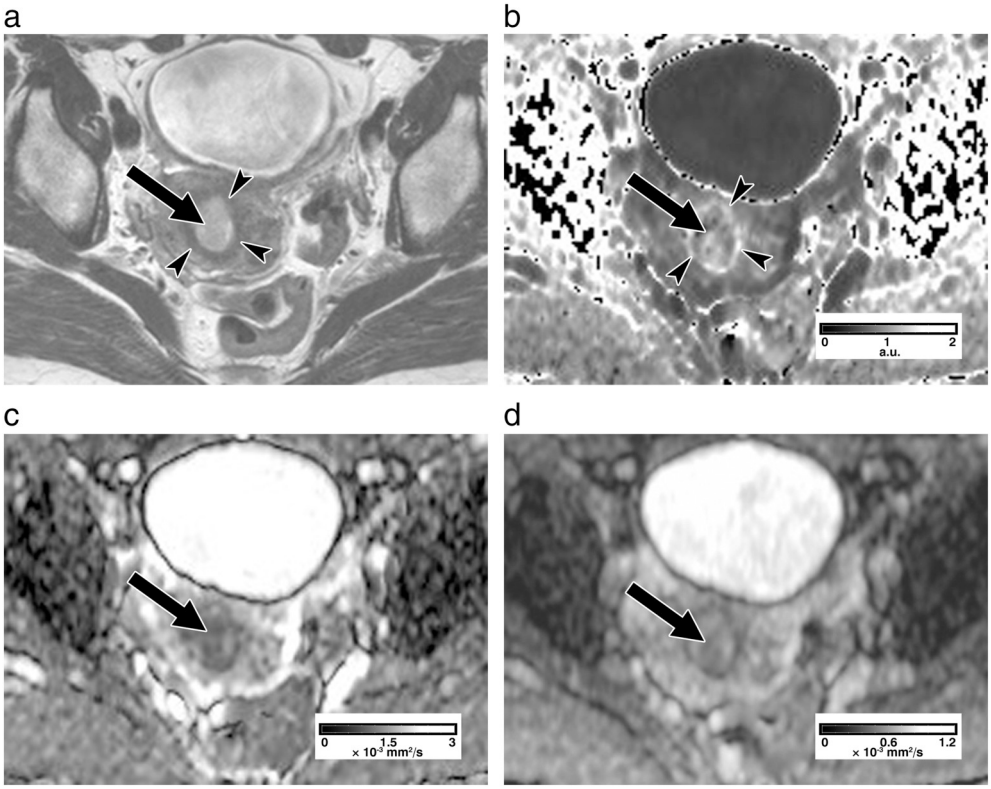

Fig. 1. Images of a 48-year-old woman with EMC showing stage IA and grade 1 EMAC.
(a) T2WI shows that there's a hyperintense mass lesion (arrow) confined to EM and that the hypointense JZ (arrowheads) is intact.
(b) K map shows that the mass lesion (arrow) has intermediate K values and that the high-K JZ (arrowheads) is intact. (a.u. = arbitrary units).
(c) D map shows that the mass lesion (arrow) has low D values.
(d) ADC map shows that the mass lesion (arrow) has low ADC values.

3. Results

3.1. Uterine wall layers on DKI maps

As shown in Fig. 1, K and D maps of all patients (100%) clearly depicted the uterine wall as consisting of the following three layers: endometrium (EM); junctional zone (JZ); and outer myometrium (OMM). These three layers seemed to correspond well with the uterine wall layers observed on T2WI. Particularly, K maps showed JZ as a high-K zone distinct from EM and OMM.

In all patients, K values of JZ (1.443 ± 0.362) were significantly higher than those of EM and OMM (0.678 ± 0.179 and 0.694 ± 0.113, respectively; $P < 0.001$ for both; Table 1). High-K JZ showed the highest deviation of diffusion from Gaussian behavior in the uterine wall [21,22] perhaps because of anisotropic local fiber orientation in JZ [25]. These results demonstrate that K maps could clearly differentiate JZ from EM and OMM in patients with EMC.

3.2. DKI parameters of EMCs and uterine wall layers

In 22 EMC cases, K values were 1.048 ± 0.145 a.u., D values were 1.068 ± 0.160 × 10^{-3} mm^2/s, and ADC values were 0.618 ± 0.066 × 10^{-3} mm^2/s (Table 1). D values of EMCs were significantly larger than ADC values ($P < 0.001$) because D value represented the diffusion coefficient corrected for the non-Gaussian bias [21,22], thereby demonstrating that the effect of non-Gaussian diffusion considerably contributed to D values of the EMCs. Similarly, higher K values of EMCs implied a greater deviation of diffusion from the Gaussian behavior because a K value of 0 indicates a perfectly Gaussian diffusion [21,22].

K values from all 22 EMCs were significantly lower than those from JZ ($P < 0.001$) while the EMC K values were significantly higher than those from EM and OMM ($P < 0.001$ for both) (Table 1 and Fig. 2). On D maps, all 22 EMCs showed significantly lower D values than all normal uterine wall layers ($P < 0.001$ for EM, $P = 0.048$ for JZ, and $P < 0.001$ for OMM). In contrast, ADC values of EMCs were significantly lower than were those of EM and OMM ($P < 0.001$ for both), but there were no significant differences in ADC values between EMCs and JZ ($P = 0.588$).

Further, K values of EMC (1.048 ± 0.145 a.u.) were significantly higher than those of the normal EM (0.678 ± 0.179 a.u.; $P < 0.001$), which served as the control group for the comparison of EMC and EM. These results indicate that the kurtosis changes were resulting form EMC itself, not from myometrial fiber orientation. This is probably because the presence of both barriers (e.g. cell membranes) and compartments (e.g. intracellular and extracellular spaces) within EMC could alter the water displacement probability distribution function compared with the normal EM.

These data demonstrate that EMCs and normal uterine wall could be clearly demarcated for DKI maps.

Table 1
K, D, and ADC values of the normal uterine wall layers and endometrial carcinomas.

Tissue	K values (a.u.)	D values ($\times 10^{-3}$ mm^2/s)	ADC values ($\times 10^{-3}$ mm^2/s)
Endometrium	0.678 ± 0.179[a]	2.450 ± 0.629[a]	1.185 ± 0.305[a]
Junctional zone	1.443 ± 0.362[a]	1.420 ± 0.191[a]	0.697 ± 0.169
Outer myometrium	0.694 ± 0.113[a]	2.644 ± 0.332[a]	1.050 ± 0.140[a]
Endometrial carcinoma	1.048 ± 0.145	1.068 ± 0.160	0.618 ± 0.066

Note: Data are mean values ± standard deviations. K = kurtosis, D = diffusivity, ADC = apparent diffusion coefficient. a.u. = arbitrary units.
[a] = Significantly different from the corresponding value of the endometrial carcinomas.

3.3. Depth of tumor invasion on DKI maps

Histopathological examination based on FIGO staging system revealed that 22 EMCs comprised 13 carcinomas in stage IA, 3 carcinomas in stage IB, 2 carcinomas in stage II, 1 carcinoma in stage IIIC1, 2 carcinomas in stage IIIC2, and 1 carcinoma in stage IVB. All EMCs were

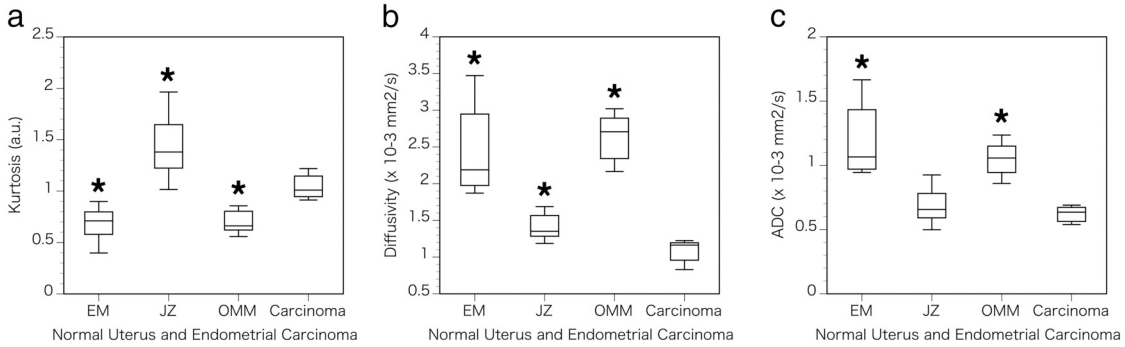

Fig. 2. Box plots of DKI parameters in normal uterine wall layers and EMCs.
(a) Comparison of K values between uterine wall layers and EMCs. K values of EMCs were significantly lower than those of JZ and were significantly higher than those of EM and OMM. * = Significant difference ($P < 0.001$).
(b) Comparison of D values between uterine wall layers and EMCs. EMCs showed significantly lower D values than all normal uterine wall layers. * = Significant difference ($P < 0.001$ for EM, $P = 0.048$ for JZ, and $P < 0.001$ for OMM).
(c) Comparison of ADC values between uterine wall layers and EMCs. ADC values of EMCs were significantly lower than those of EM and OMM, but there were no significant differences between EMCs and JZ. * = Significant difference ($P < 0.001$).

clearly depicted as intermediate K areas on K maps and as low D areas on D maps. Thus, the same depth of tumor invasion into the myometrium could be depicted on DKI maps compared with histopathological examination.

EMCs confined to EM appeared as localized masses with intermediate K and low D values and intact high-K JZ on DKI maps (Fig. 1). In contrast, EMCs that invaded the myometrium appeared as masses with intermediate K and low D values and disrupted myometrial high-K JZ on DKI maps (Fig. 3). Notably, JZ was clearly depicted on K maps but not on T2WI (Fig. 3). These findings demonstrate that K maps may be more useful for depicting JZ than T2WI because T2WI often cannot depict JZ in postmenopausal patients and depending on the menstrual cycle.

3.4. Histological grades of EMCs on DKI maps

We investigated the association of the histological grades of EMCs with DKI parameters. Histopathological examination revealed that 22 EMCs comprised 15 endometrioid adenocarcinomas (EMACs), 3 serous adenocarcinomas, 1 clear cell adenocarcinoma, 2 mixed carcinomas, and 1 carcinosarcoma. Among the 15 EMACs, 10 carcinomas were grade 1, 4 carcinomas were grade 2, and 1 carcinoma was grade 3.

We combined grade 2 and grade 3 cases into “high-grade group” (5 cases) and grade 1 cases into “low-grade group” (10 cases). K values of the high-grade group were significantly higher than those of the low-grade group (1.203 ± 0.130 a.u. vs. 0.970 ± 0.071 a.u.; $P = 0.001$). D values of the high-grade group were significantly lower than those of the low-grade group ($0.884 \pm 0.107 \times 10^{-3}$ mm^2/s vs. $1.161 \pm 0.078 \times 10^{-3}$ mm^2/s; $P = 0.001$). However, ADC values between the high-grade and low-grade groups were not significantly different ($0.607 \pm 0.063 \times 10^{-3}$ mm^2/s vs. $0.634 \pm 0.053 \times 10^{-3}$ mm^2/s; $P = 0.440$).

Further, K values showed a significant positive correlation with the histological grades ($r = 0.799$; $P < 0.001$) (Table 2 and Fig. 4). Similarly, D values showed a significant inverse correlation with the histological grades ($r = -0.799$; $P < 0.001$). However, no significant correlation was found between ADC values and histological grades ($r = -0.243$; $P = 0.382$).

Representative cases with grade 1 and grade 2 EMACs are shown in Figs. 3 and 5 respectively. These results indicate that histological grades of EMCs could be differentiated on the basis of DKI parameters.

3.5. Lymph node metastasis on DKI maps

Next, we investigated the association between lymph node status in patients with EMC and DKI parameters. Lymph node metastasis was found in 4 of the 22 patients with EMC; each histologically confirmed lymph node (5 metastatic and 11 nonmetastatic) was compared with DKI parameters on a node-by-node basis.

K values of metastatic lymph nodes were significantly higher than those of nonmetastatic lymph nodes (1.173 ± 0.112 a.u. vs. 0.929 ± 0.076 a.u.; $P = 0.001$) (Table 3 and Fig. 6). Similarly, D values of metastatic lymph nodes were significantly lower than those of nonmetastatic lymph nodes ($1.221 \pm 0.108 \times 10^{-3}$ mm^2/s vs. $1.547 \pm 0.153 \times 10^{-3}$ mm^2/s; $P = 0.001$). However, ADC values between metastatic and nonmetastatic lymph nodes were not significantly different ($0.634 \pm 0.033 \times 10^{-3}$ mm^2/s vs. $0.646 \pm 0.019 \times 10^{-3}$ mm^2/s; $P = 0.827$).

Representative cases with nonmetastatic and metastatic lymph nodes are shown in Figs. 7 and 8, respectively. These results indicate that metastatic and nonmetastatic lymph nodes in patients with EMC could be differentiated on the basis of DKI parameters.

3.6. ROC curve analyses of DKI parameters

Results of ROC curve analyses for differentiating grade 2 or 3 EMACs from grade 1 EMACs are shown in Table 4 and Fig. 9a. Compared with areas under the curve (AUCs) for ADC values (0.640), AUCs for K (0.980; $P = 0.0425$) and D (0.980; $P = 0.0442$) values were significantly larger. AUCs for K and D values ($P = 1.000$) were not significantly different. Therefore, a cutoff K value of > 1.012 a.u. and a cutoff D value of $\leq 1.025 \times 10^{-3}$ mm^2/s seem to be useful for differentiating grade 2 or grade 3 EMACs from grade 1 EMACs.

Results of ROC curve analyses for differentiating metastatic and nonmetastatic lymph nodes in patients with EMC are shown in Table 5 and Fig. 9b. AUCs for K (0.982; $P = 0.0297$) and D (0.982; $P = 0.0494$) values were significantly larger than AUCs for ADC (0.545). AUCs between K and D values ($P = 1.000$) were not significantly different. Therefore, a cutoff K value of > 0.994 a.u. and a cutoff D value of $\leq 1.400 \times 10^{-3}$ mm^2/s seem to be useful for differentiating metastatic and nonmetastatic lymph nodes in patients with EMC.

4. Discussion

Conventional DWI parameters assume a Gaussian behavior of water diffusion; thus, the distribution of water displacement follows a statistically similar distribution to free diffusion, and SI attenuations in DWI are monoexponential with the b values used. However, the complex structure of most tissues, which comprise various types of cells and cell membranes, can cause a substantial deviation of the distribution of

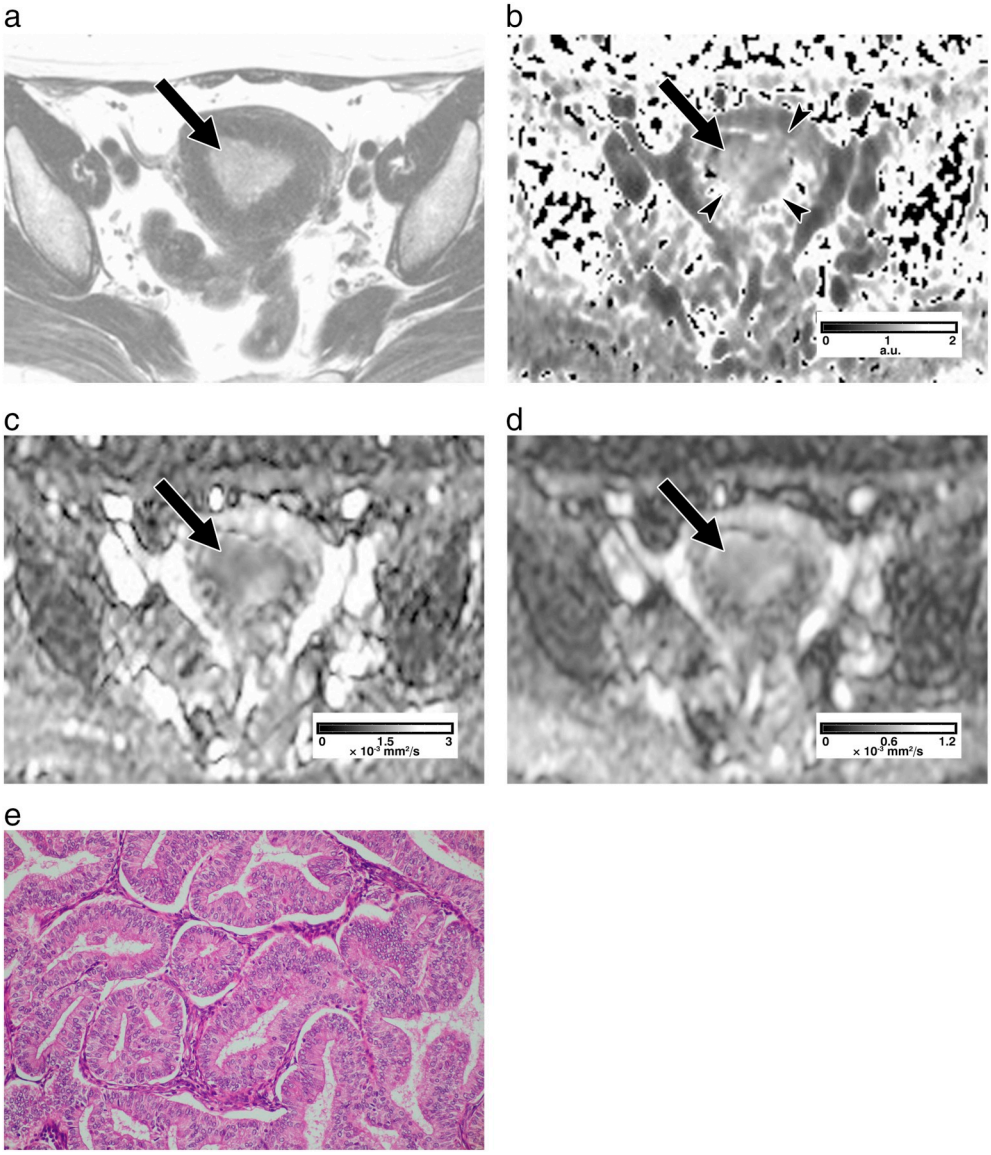

Fig. 3. Images of a 49-year-old woman with EMC showing stage IA and grade 1 EMAC.
(a) T2WI shows that there's a hyperintense mass lesion (arrow) in EM, although JZ is not clearly depicted on T2WI.
(b) K map shows that the mass lesion (arrow) has intermediate K values (0.960 a.u.) and that the high-K JZ (arrowheads) has been partially disrupted. (a.u. = arbitrary units).
(c) D map shows that the mass lesion (arrow) has low D values (1.188×10^{-3} mm^2/s).
(d) ADC map shows that the mass lesion (arrow) has low ADC values (0.636×10^{-3} mm^2/s).
(e) Histopathological examination shows well-differentiated EMAC (grade 1). (H-E stain; original magnification, ×200).

diffusion displacement from a Gaussian behavior. As a non-Gaussian model of DWI, DKI was first proposed for investigating neurologic pathologies [21]. Since DKI can quantify the deviation of diffusion from a Gaussian behavior, it can more accurately reflect the microstructural complexities of tissues than can conventional DWI [21,22]. DKI-derived parameters are associated with histological grades of gliomas and prostate and breast cancers [15–19]. Recently, Yamada et al. [20] have demonstrated that DKI was useful for evaluating histological grade and lymph node metastasis in patients with oral carcinoma. Moreover, they [26,27] have demonstrated that q-space imaging (QSI)—another non-Gaussian model of DWI—is useful for ex vivo evaluation of tumor invasion depth, histological grade, and lymph node metastasis in esophageal and gastric carcinomas. Therefore, we hypothesized that DKI might be more effective than conventional DWI for the assessment of tumor invasion depth, histological grade, and lymph node metastasis in patients with EMC.

Our findings demonstrated that K maps of all patients clearly depicted JZ as a distinct high-K zone that was significantly different from EM and OMM. As K values quantify the deviation of diffusion from the Gaussian behavior, such a high-K value in JZ indicates that JZ showed the highest deviation of diffusion from Gaussian behavior in the uterine wall. In a recent study, Yamada et al. [25] have used diffusion-tensor

Table 2
K, D, and ADC values in the histological grades of endometrioid adenocarcinomas.

Histological grades	K values (a.u.)	D values ($\times 10^{-3}$ mm^2/s)	ADC values ($\times 10^{-3}$ mm^2/s)
Grade 1 (n = 10)	0.970 ± 0.071[a]	1.161 ± 0.078[a]	0.634 ± 0.053
Grade 2 (n = 4)	1.152 ± 0.069	0.918 ± 0.087	0.613 ± 0.072
Grade 3 (n = 1)	1.409	0.748	0.585

Note: Data are mean values ± standard deviations. K = kurtosis, D = diffusivity, ADC = apparent diffusion coefficient. Grade 1 = well differentiated, Grade 2 = moderately differentiated, Grade 3 = poorly differentiated. a.u. = arbitrary units.
[a] = Significantly different for the histological grades of the endometrioid adenocarcinomas ($P < 0.001$).

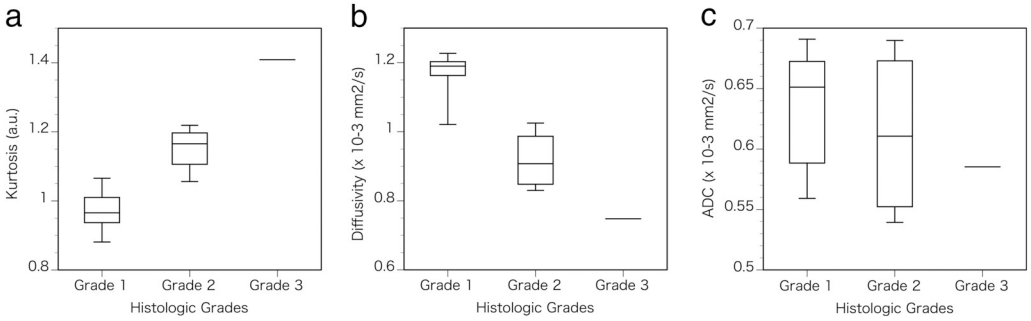

Fig. 4. Box plots of DKI parameters in the histological grades of EMACs.
(a) Comparison of K values in different histological grades of EMACs showing a significant positive correlation ($r = 0.799$; $P < 0.001$).
(b) Comparison of D values in different histological grades of EMACs showing a significant inverse correlation ($r = -0.799$; $P < 0.001$).
(c) Comparison of ADC values in different histological grades of EMACs showing no significant correlation ($r = -0.243$; $P = 0.382$).

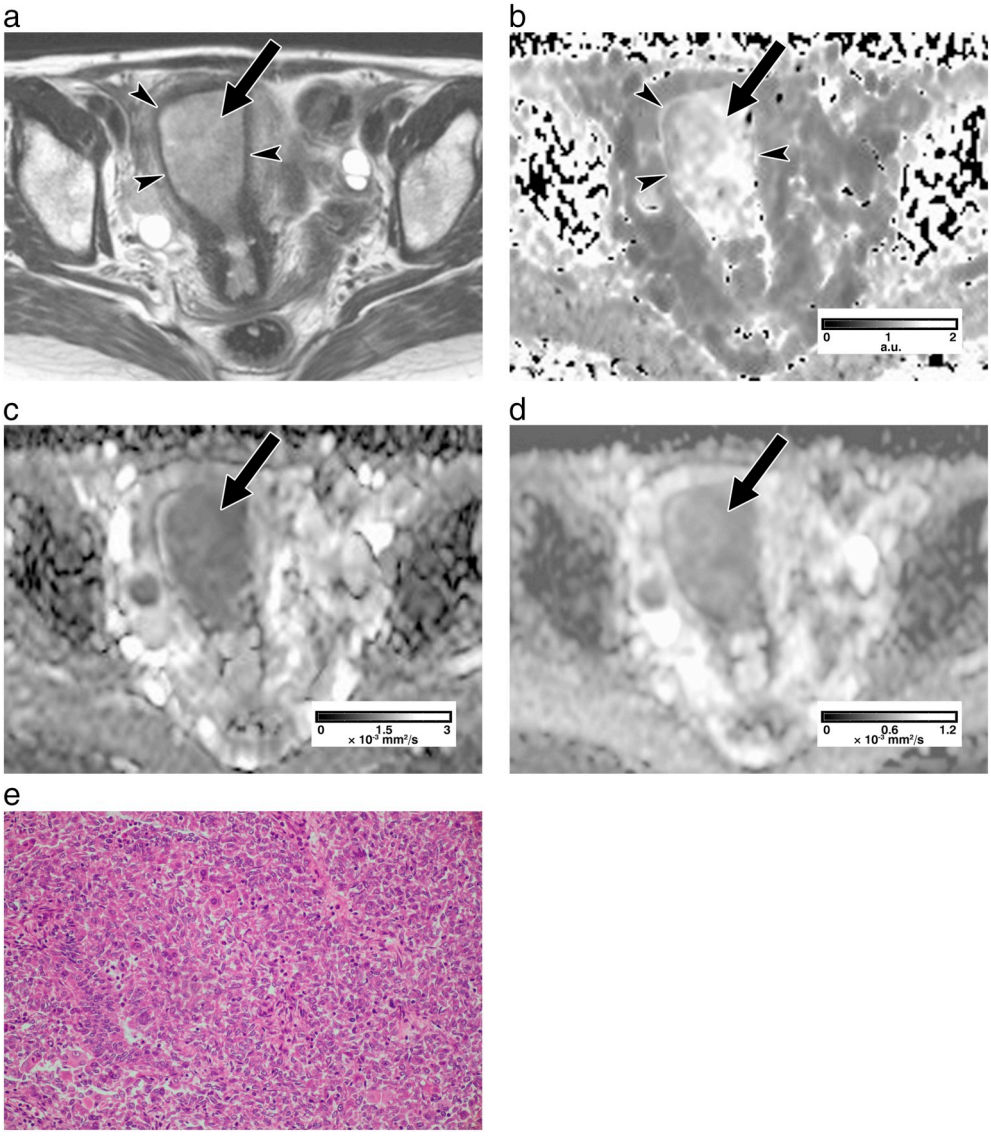

Fig. 5. Images of a 49-year-old woman with EMC showing stage IA and grade 2 EMAC.
(a) T2WI shows that there's a hyperintense mass lesion (arrow) confined to EM and that the hypointense JZ (arrowheads) is intact.
(b) K map shows that the mass lesion (arrow) has high K values (1.156 a.u.) and that the high-K JZ (arrowheads) is intact. (a.u. = arbitrary units).
(c) D map shows that the mass lesion (arrow) has low D values ($0.866 \times 10^{-3}\,mm^2/s$).
(d) ADC map shows that the mass lesion (arrow) has low ADC values ($0.611 \times 10^{-3}\,mm^2/s$).
(e) Histopathological examination shows moderately differentiated EMAC (grade 2). (H-E stain; original magnification, ×200).

Table 3
K, D, and ADC values of metastatic and nonmetastatic lymph nodes in patients with endometrial carcinoma.

Lymph nodes	K values (a.u.)	D values ($\times 10^{-3}\,mm^2/s$)	ADC values ($\times 10^{-3}\,mm^2/s$)
Nonmetastatic (n = 11)	0.929 ± 0.076[a]	1.547 ± 0.153[a]	0.646 ± 0.019
Metastatic (n = 5)	1.173 ± 0.112	1.221 ± 0.108	0.634 ± 0.033

Note: Data are mean values ± standard deviations. K = kurtosis, D = diffusivity, ADC = apparent diffusion coefficient. a.u. = arbitrary units.
[a] = Significantly different between metastatic and nonmetastatic lymph nodes in patients with endometrial carcinoma (P = 0.001).

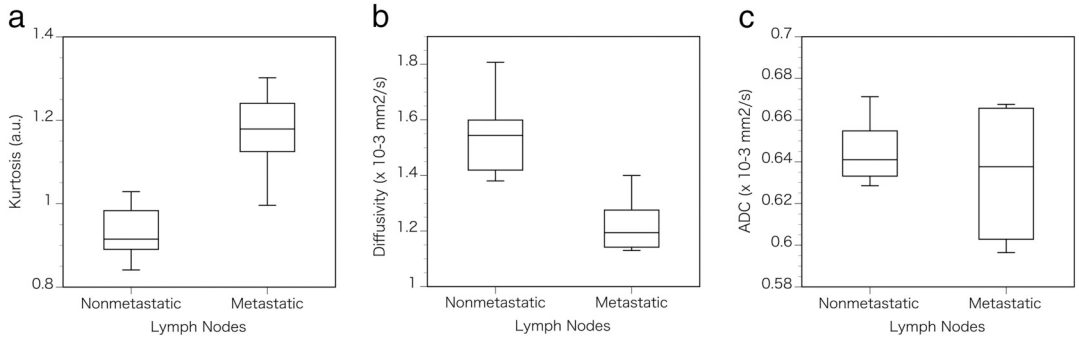

Fig. 6. Box plots of the DKI parameters in nonmetastatic and metastatic lymph nodes in patients with EMC.
(a) Comparison of the K values between nonmetastatic and metastatic lymph nodes showing significant differences (P = 0.001).
(b) Comparison of the D values between nonmetastatic and metastatic lymph nodes showing significant differences (P = 0.001).
(c) Comparison of the ADC values between nonmetastatic and metastatic lymph nodes showing no significant differences (P = 0.827).

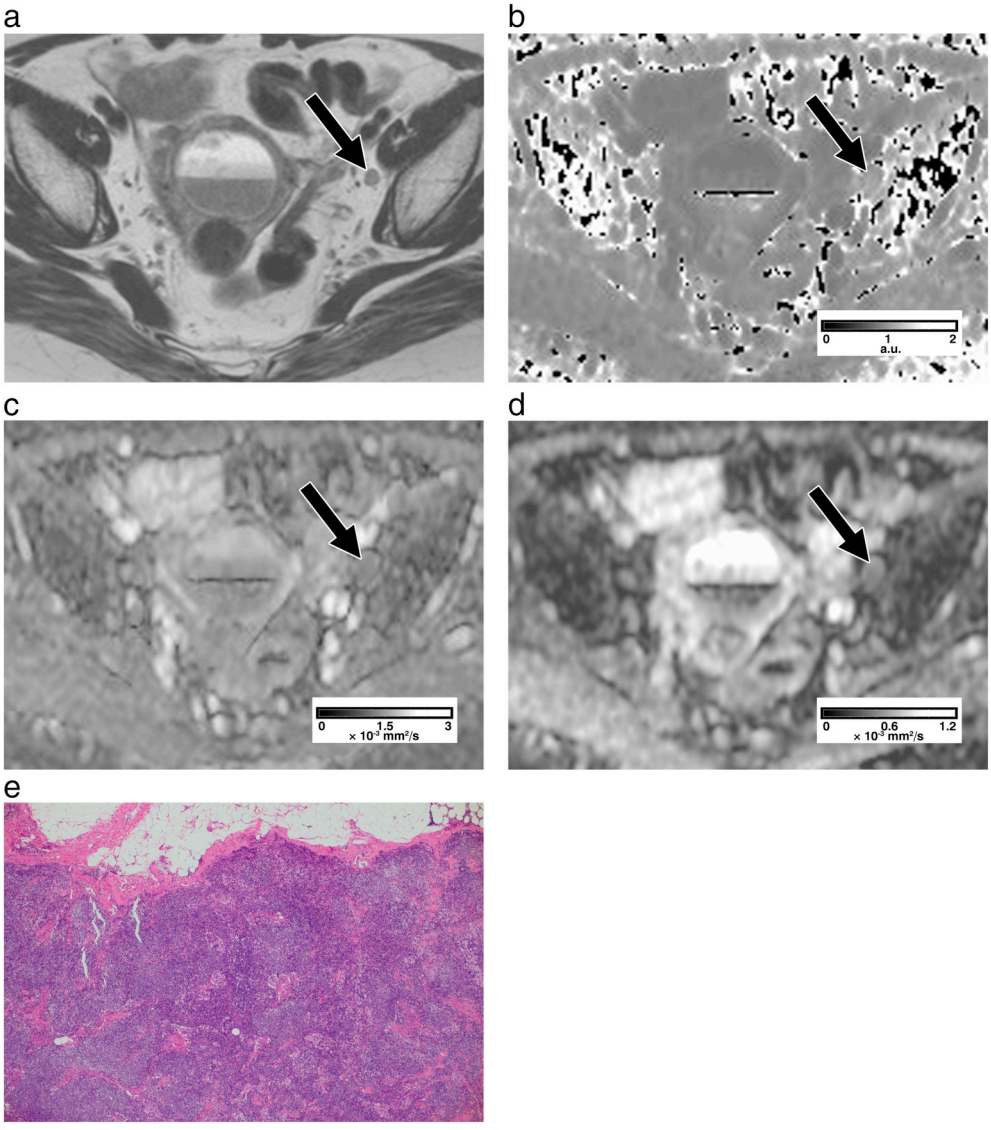

Fig. 7. Images of a 65-year-old woman with nonmetastatic lymph nodes. This patient had EMC and hematometra; the DKI data acquisition was performed before contrast enhancement MRI as usual.
(a) T2WI shows a swollen lymph node (arrow) in the left obturator region.
(b) K map shows that the lymph node (arrow) is slightly hyperintense (K = 0.915 a.u.). (a.u. = arbitrary units).
(c) D map shows that the lymph node (arrow) is slightly hypointense ($D = 1.544 \times 10^{-3}\,mm^2/s$).
(d) ADC map shows that the lymph node (arrow) is slightly hypointense ($ADC = 0.641 \times 10^{-3}\,mm^2/s$).
(e) Histopathological examination shows that the lymph node has no metastasis. (H-E stain; original magnification, ×40).

imaging (DTI) and demonstrated that JZ constituted densely packed, parallel-oriented smooth muscle fibers to EM, whereas OMM constituted less dense, randomly oriented smooth muscle fibers. Therefore, high-K in JZ seems to be due to anisotropic local fiber orientation. Although previous reports have demonstrated zonal differences in the normal uterus on DTI maps [28,29], to the best of our knowledge, the present study is the first to reveal the association between DKI parameters and zonal differences of the normal uterus.

In the present study involving 22 EMC cases, non-Gaussian D values of EMCs were significantly larger than conventional Gaussian ADC values. Because D value represents the diffusion coefficient corrected for a non-Gaussian bias [21,22], these data demonstrate the substantial

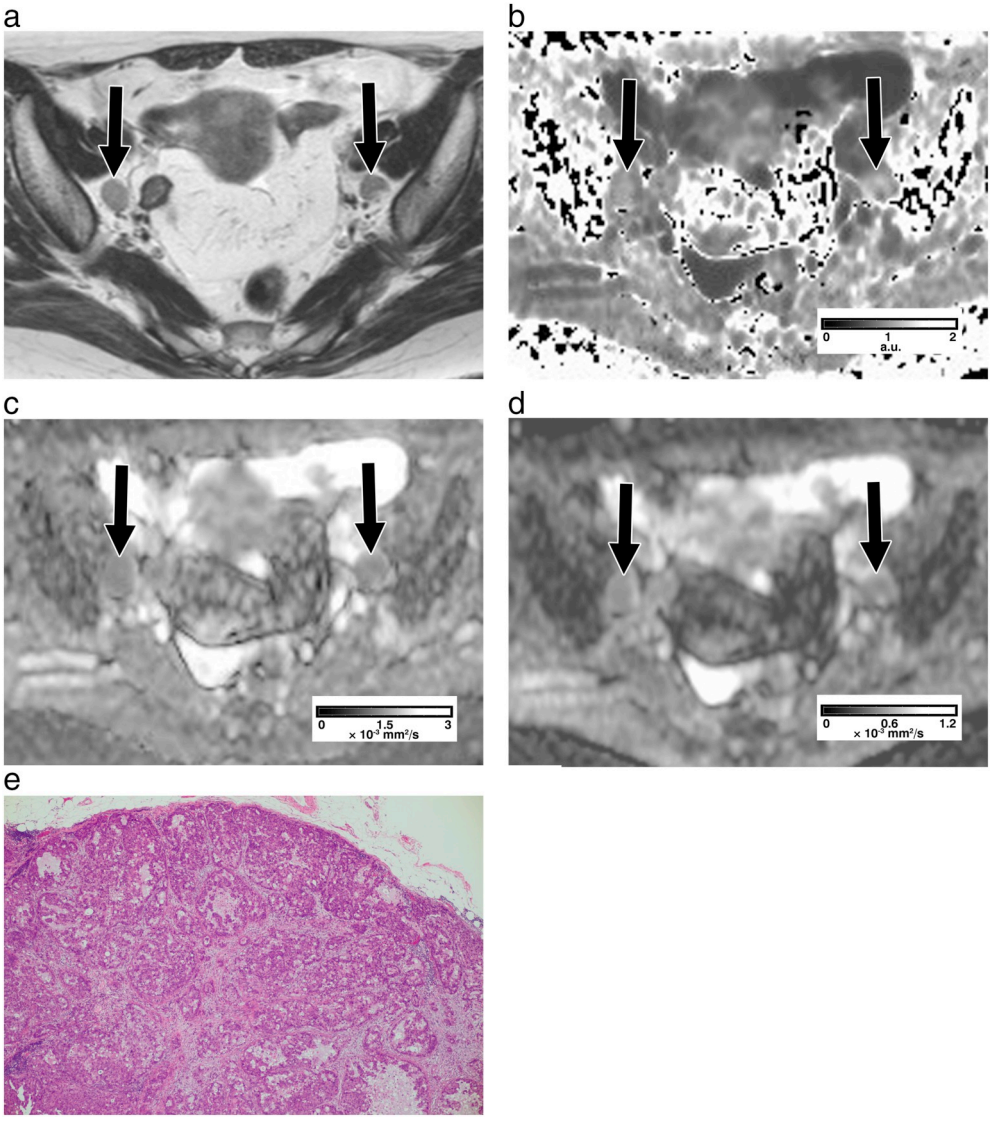

Fig. 8. Images of a 60-year-old woman with metastatic lymph nodes.
(a) T2WI shows swollen lymph nodes (arrows) in the bilateral obturator region.
(b) K map shows that the lymph nodes (arrows) are hyperintense (right side: K = 1.168 a.u.; left side: K = 1.179 a.u.). (a.u. = arbitrary units).
(c) D map shows that the lymph nodes (arrows) are slightly hypointense (right side: D = 1.234×10^{-3} mm^2/s; left side: 1.194×10^{-3} mm^2/s).
(d) ADC map shows that the lymph nodes (arrows) are slightly hypointense (right side: ADC = 0.638×10^{-3} mm^2/s; left side: ADC = 0.605×10^{-3} mm^2/s).
(e) Histopathological examination shows that the lymph nodes have metastasis of endometrial carcinoma. (H-E stain; original magnification, ×40).

Table 4
ROC curve analyses of K, D, and ADC values for differentiating grade 2 or grade 3 from grade 1 endometrioid adenocarcinomas.

Parameter	AUC	Optimal threshold	Sensitivity (%)	Specificity (%)	P value
K values	0.980	> 1.012 (a.u.)	100.00 (5/5)	90.00 (9/10)	0.0425
D values	0.980	≤1.025 ($\times 10^{-3}$ mm^2/s)	100.00 (5/5)	90.00 (9/10)	0.0442
ADC values	0.640	≤0.585 ($\times 10^{-3}$ mm^2/s)	60.00 (3/5)	80.00 (8/10)	NA

Note: Optimal threshold of each parameter was determined to maximize average of sensitivity and specificity. Data in parentheses are numbers used to calculate percentages. P value represents differences in comparison with performance of ADC. AUC = area under the curve. K = kurtosis, D = diffusivity, ADC = apparent diffusion coefficient. a.u. = arbitrary units. NA = not available.

contribution of the effect of non-Gaussian diffusion to D values of EMCs. Similarly, since a K value of zero indicates perfect Gaussian diffusion [21,22], higher K values of EMCs imply a greater deviation of diffusion from the Gaussian behavior. These tendencies are consistent with those reported in previous studies on other organs [17]. Moreover, a significant increase in D values compared with ADC values has been observed in various other tissues [17–19].

We found that K values from all 22 EMCs were significantly lower than those from JZ while the EMC K values were significantly higher than those from EM and OMM. On D maps, all 22 EMCs had significantly lower D values than all normal uterine wall layers. Accordingly, all EMCs were clearly demarcated from the normal uterine wall on K and D maps, indicating that the same depth of tumor invasion into the myometrium could be determined on DKI maps compared with histological examination. Importantly, JZ was clearly depicted on K maps although JZ was not depicted by T2WI. Therefore, K maps may be more useful for depicting JZ than is T2WI. T2WI is frequently unable to depict JZ in postmenopausal patients, and this ability also depends on the menstrual cycle. Although previous reports have shown that DTI may be a useful tool for the diagnosis of myometrial invasion of EMC

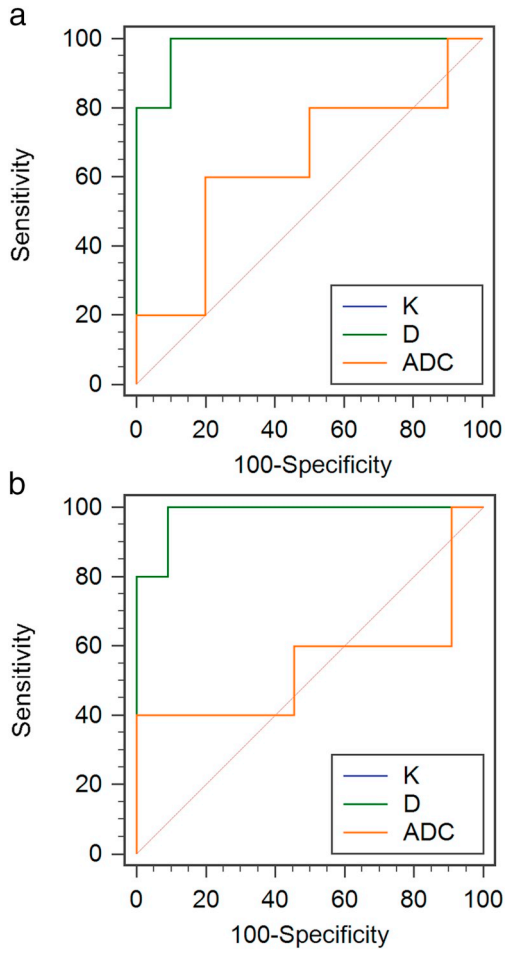

Fig. 9. ROC curve analyses of DKI parameters in patients with EMC.
(a) ROC curves for differentiating grade 2 or grade 3 EMACs from grade 1 EMACs. AUCs for K (0.980; P = 0.0425) and D (0.980; P = 0.0442) values were significantly larger than AUCs for ADC values (0.640). There were no significant differences in AUCs between K and D values (P = 1.000).
(b) ROC curves for differentiating metastatic and nonmetastatic lymph nodes in patients with EMC. AUCs for K (0.982; P = 0.0297) and D (0.982; P = 0.0494) values were significantly larger than AUCs for ADC values (0.545). There were no significant differences in AUCs between K and D values (P = 1.000).

[25,30,31], the present study, to the best of our knowledge, is the first to reveal the usefulness of DKI for the depth of myometrial tumor invasion in patients with EMC.

Furthermore, our data have revealed significant correlations between DKI parameters and histological grades of EMCs. Previous studies have shown that DKI parameters are associated with histological grades of cerebral gliomas and prostate and breast cancers [15–19]. In particular, K values tend to be higher with increasing malignant behavior perhaps because of the intratumoral heterogeneity in addition to increasing cellular density [17]. Since DKI is very sensitive to changes in microstructural organization [21,22], it could be an effective method for the noninvasive assessment of histological grades of EMCs. Previous studies have shown that differentiation among histological grades of EMCs based on ADC values is often difficult because of the considerable overlap among ADC values of different histological grades [8–14]. Therefore, DKI seems to be more accurate than conventional DWI in differentiating histological grades of EMCs. As such, a recent report has demonstrated that DKI is relatively better than DWI in distinguishing high- and low-grade EMCs [32].

Our findings have demonstrated that DKI can differentiate between metastatic and nonmetastatic lymph nodes in patients with EMC. Previous reports have indicated that the evaluation of lymph node metastasis in patients with EMC is challenging with any imaging modality because nodal size alone is not a reliable diagnostic criterion for lymph node metastasis [5–7]. Similar to the aforementioned limitations of ADC values in the evaluation of histological tumor grades, results of recent studies have shown that differentiation between metastatic and nonmetastatic lymph nodes based on ADC values is likely difficult for the same reasons [33,34]. However, DKI might be a useful tool for the noninvasive assessment of lymph node metastasis in patients with EMC because it is potentially sensitive to aspects of the microstructural complexity of the tissue.

Our study had two limitations. First, the study cohort was relatively small for defining differences in DKI parameters among different histological grades. Nevertheless, we obtained significant thresholds to differentiate between different histological grades. We believe that these findings need further validation in a larger study involving more patients with EMC.

Second, the number of b values (0, 500, 1000, and 2000 s/mm^2) used for estimating DKI parameters was relatively smaller than that used in previous reports. This may have affected the curve fitting of DKI data; however, the calculated DKI parameters were consistent with those reported in previous studies [17,18]. Our ultimate goal would be the routine application of DKI as a noninvasive quantitative tool for accurate preoperative evaluation and selection of optimal therapy within a clinically feasible duration for patients with EMC.

In conclusion, K maps showed JZ as a distinct high-K zone that was significantly different from EM and OMM. All EMCs were clearly demarcated from the normal uterine wall on DKI maps. K and D values were significantly correlated with histological grades of EMCs and were significantly different between metastatic and nonmetastatic lymph nodes in patients with EMC. Therefore, DKI can potentially provide useful information for evaluating the depth of tumor invasion, histological grade of EMCs, and presence of lymph node metastasis in patients with EMC.

Table 5
ROC curve analyses of K, D, and ADC values for differentiating metastatic from nonmetastatic lymph nodes in patients with endometrial carcinomas.

Parameter	AUC	Optimal threshold	Sensitivity (%)	Specificity (%)	P value
K values	0.982	> 0.994 (a.u.)	100.00 (5/5)	90.91 (10/11)	0.0297
D values	0.982	≤1.400 ($\times 10^{-3}$ mm^2/s)	100.00 (5/5)	90.91 (10/11)	0.0494
ADC values	0.545	≤0.605 ($\times 10^{-3}$ mm^2/s)	40.00 (2/5)	100.00 (11/11)	NA

Note: Optimal threshold of each parameter was determined to maximize average of sensitivity and specificity. Data in parentheses are numbers used to calculate percentages. P value represents differences in comparison with performance of ADC. AUC = area under the curve. K = kurtosis, D = diffusivity, ADC = apparent diffusion coefficient. a.u. = arbitrary units. NA = not available.

Acknowledgment

We thank Shinya Ayabe, MT, for his technical contributions and assistance.

Conflicts of interest and sources of funding

For all the authors listed, no conflicts are declared. Dr. Yamada has received the Grant-in-Aid for Scientific Research (C) of MEXT, Japan (15K09915).

References

[1] Siegel R, Naishadham D, Jemal A. Cancer statistics, 2013. CA Cancer J Clin 2013;63:11–30.
[2] Prat J. Prognostic parameters of endometrial carcinoma. Hum Pathol 2004;35:649–62.
[3] Arora V, Quinn MA. Endometrial cancer. Best Pract Res Clin Obstet Gynaecol 2012;26:311–24.
[4] Larson DM, Connor GP, Broste SK, Krawisz BR, Johnson KK. Prognostic significance of gross myometrial invasion with endometrial cancer. Obstet Gynecol 1996;88:394–8.
[5] Manfredi R, Mirk P, Maresca G, Margariti PA, Testa A, Zannoni GF, et al. Local-regional staging of endometrial carcinoma: role of MR imaging in surgical planning. Radiology 2004;231:372–8.
[6] Nagar H, Dobbs S, McClelland HR, Price J, McCluggage WG, Grey A. The diagnostic accuracy of magnetic resonance imaging in detecting cervical involvement in endometrial cancer. Gynecol Oncol 2006;103:431–4.
[7] Beddy P, O'Neill AC, Yamamoto AK, Addley HC, Reinhold C, Sala E. FIGO staging system for endometrial cancer: added benefits of MR imaging. Radiographics 2012;32:241–54.
[8] Tamai K, Koyama T, Saga T, Umeoka S, Mikami Y, Fujii S, et al. Diffusion-weighted MR imaging of uterine endometrial cancer. J Magn Reson Imaging 2007;26:682–7.
[9] Rechichi G, Galimberti S, Signorelli M, Franzesi CT, Perego P, Valsecchi MG, et al. Endometrial cancer: correlation of apparent diffusion coefficient with tumor grade, depth of myometrial invasion, and presence of lymph node metastases. AJR Am J Roentgenol 2011;197:256–62.
[10] Seo JM, Kim CK, Choi D, Kwan Park B. Endometrial cancer: utility of diffusion-weighted magnetic resonance imaging with background body signal suppression at 3 T. J Magn Reson Imaging 2013;37:1151–9.
[11] Woo S, Cho JY, Kim SY, Kim SH. Histogram analysis of apparent diffusion coefficient map of diffusion-weighted MRI in endometrial cancer: a preliminary correlation study with histological grade. Acta Radiol 2014;55:1270–7.
[12] Inoue C, Fujii S, Kaneda S, Fukunaga T, Kaminou T, Kigawa J, et al. Correlation of apparent diffusion coefficient value with prognostic parameters of endometrioid carcinoma. J Magn Reson Imaging 2015;41:213–9.
[13] Nougaret S, Reinhold C, Alsharif SS, Addley H, Arceneau J, Molinari N, et al. Endometrial cancer: combined MR volumetry and diffusion-weighted imaging for assessment of myometrial and lymphovascular invasion and tumor grade. Radiology 2015;276:797–808.
[14] Bakir VL, Bakir B, Sanli S, Yildiz SO, Iyibozkurt AC, Kartal MG, et al. Role of diffusion-weighted MRI in the differential diagnosis of endometrioid and non-endometrioid cancer of the uterus. Acta Radiol 2017;58:758–67.
[15] Raab P, Hattingen E, Franz K, Zanella FE, Lanfermann H. Cerebral gliomas: diffusional kurtosis imaging analysis of microstructural differences. Radiology 2010;254:876–81.
[16] Van Cauter S, Veraart J, Sijbers J, Peeters RR, Himmelreich U, De Keyzer F, et al. Gliomas: diffusion kurtosis MR imaging in grading. Radiology 2012;263:492–501.
[17] Rosenkrantz AB, Sigmund EE, Johnson G, Babb JS, Mussi TC, Melamed J, et al. Prostate cancer: feasibility and preliminary experience of a diffusional kurtosis model for detection and assessment of aggressiveness of peripheral zone cancer. Radiology 2012;264:126–35.
[18] Rosenkrantz AB, Padhani AR, Chenevert TL, Koh DM, De Keyzer F, Taouli B, et al. Body diffusion kurtosis imaging: basic principles, applications, and considerations for clinical practice. J Magn Reson Imaging 2015;42:1190–202.
[19] Sun K, Chen X, Chai W, Fei X, Fu C, Yan X, et al. Breast cancer: diffusion kurtosis MR imaging-diagnostic accuracy and correlation with clinical-pathologic factors. Radiology 2015;277:46–55.
[20] Yamada I, Yoshino N, Hikishima K, Sakamoto J, Yokokawa M, Oikawa Y, et al. Oral carcinoma: clinical evaluation using diffusion kurtosis imaging and its correlation with histopathologic findings. Magn Reson Imaging 2018;51:69–78.
[21] Jensen JH, Helpern JA, Ramani A, Lu H, Kaczynski K. Diffusional kurtosis imaging: the quantification of non-Gaussian water diffusion by means of magnetic resonance imaging. Magn Reson Med 2005;53:1432–40.
[22] Jensen JH, Helpern JA. MRI quantification of non-Gaussian water diffusion by kurtosis analysis. NMR Biomed 2010;23:698–710.
[23] Sakamoto J, Kuribayashi A, Kotaki S, Fujikura M, Nakamura S, Kurabayashi T. Application of diffusion kurtosis imaging to odontogenic lesions: analysis of the cystic component. J Magn Reson Imaging 2016;44:1565–71.
[24] Pecorelli S. Revised FIGO staging for carcinoma of the vulva, cervix, and endometrium. Int J Gynaecol Obstet 2009;105:103–4.
[25] Yamada I, Wakana K, Kobayashi D, Miyasaka N, Oshima N, Wakabayashi A, et al. Endometrial carcinoma: evaluation using diffusion-tensor imaging and its correlation with histopathologic findings. J Magn Reson Imaging 2018. https://doi.org/10.1002/jmri.26558.
[26] Yamada I, Hikishima K, Miyasaka N, Tokairin Y, Ito E, Kawano T, et al. Esophageal carcinoma: evaluation with q-space diffusion-weighted MR imaging ex vivo. Magn Reson Med 2015;73:2262–73.
[27] Yamada I, Hikishima K, Miyasaka N, Kato K, Ito E, Kojima K, et al. q-Space MR imaging of gastric carcinoma ex vivo: correlation with histopathologic findings. Magn Reson Med 2016;76:602–12.
[28] Fujimoto K, Kido A, Okada T, Uchikoshi M, Togashi K. Diffusion tensor imaging (DTI) of the normal human uterus in vivo at 3 tesla: comparison of DTI parameters in the different uterine layers. J Magn Reson Imaging 2013;38:1494–500.
[29] He Y, Ding N, Li Y, Li Z, Xiang Y, Jin Z, et al. 3-T diffusion tensor imaging (DTI) of normal uterus in young and middle-aged females during the menstrual cycle: evaluation of the cyclic changes of fractional anisotropy (FA) and apparent diffusion coefficient (ADC) values. Br J Radiol 2015;88:20150043.
[30] Toba M, Miyasaka N, Sakurai U, Yamada I, Eishi Y, Kubota T. Diagnostic possibility of diffusion tensor imaging for the evaluation of myometrial invasion in endometrial cancer: an ex vivo study. J Magn Reson Imaging 2011;34:616–22.
[31] Zhang L, Liu A, Zhang T, Song Q, Wei Q, Wang H. Use of diffusion tensor imaging in assessing superficial myometrial invasion by endometrial carcinoma: a preliminary study. Acta Radiol 2015;56:1273–80.
[32] Chen T, Li Y, Lu SS, Zhang YD, Wang XN, Luo CY, et al. Quantitative evaluation of diffusion-kurtosis imaging for grading endometrial carcinoma: a comparative study with diffusion-weighted imaging. Clin Radiol 2017;72. (995.e11-.e20).
[33] Levy A, Medjhoul A, Caramella C, Zareski E, Berges O, Chargari C, et al. Interest of diffusion-weighted echo-planar MR imaging and apparent diffusion coefficient mapping in gynecological malignancies: a review. J Magn Reson Imaging 2011;33:1020–7.
[34] Rechichi G, Galimberti S, Oriani M, Perego P, Valsecchi MG, Sironi S. ADC maps in the prediction of pelvic lymph nodal metastatic regions in endometrial cancer. Eur Radiol 2013;23:65–74.